AD NUMBER

AD671946

NEW LIMITATION CHANGE

TO

Approved for public release, distribution unlimited

FROM

Distribution authorized to U.S. Gov't. agencies and their contractors; Administrative/Operational Use; 24 MAY 1968. Other requests shall be referred to Naval Air Systems Command, Attn: AIR-6022, Washington, DC 20360. [No Foreign without approval].

AUTHORITY

USNASC notice, 21 May 1969

STRESS STATE IN THE COMBINED STRESS TORSION TEST

May 24, 1968

by

H. A. Kuhn

Prepared Under Contract N00019-67-C-0251
Fracture of Metals During Deformation Processing
Under Conditions of Hot Working
Naval Air Systems Command

Drexel Institute of Technology
Department of Metallurgical Engineering
Philadelphia, Pennsylvania 19104

ABSTRACT

An analysis of the stresses in the axial stress-torsion test is presented by considering the gage section as a cylinder undergoing uniform axial deformation with superimposed torsion. Calculation of the stresses requires measurement of the radial deformation and penetration of the plastic region into the notch shoulders.

The hydrostatic stress exhibits a peak within the wall of the gage section which increases with decreasing gage length. The fracture strain in room temperature tests increases with decreasing gage length when a compressive axial load is applied and decreases slightly with decreasing gage length when a tensile axial load is applied. Severe distortion and large changes in length of the gage section during hot torsion testing prevent application of the analysis to high temperature tests.

Test data are presented for hot-rolled Inconel 600 at room temperature and 1800F.

CONTENTS

INTRODUCTION

The torsion test has a number of advantages for simulating deformation processes. The chief advantage is that large plastic strains, comparable to those found in metalworking processes, can be achieved without complications to the stress state due to necking. Moreover, tests at constant and high deformation rate are made readily by twisting at a constant rotational velocity. The chief disadvantage of the torsion test is that stress, strain, and strain rate vary from the axis to the outer fiber of a solid cylindrical specimen. However, this problem can be largely eliminated by using a hollow cylindrical specimen with a relatively thin wall thickness.

The state of stress in the simple torsion test consists of pure shear, with equal tensile and compressive stresses at 45° to the shear stresses. A variation in the stress state can be achieved if axial forces, tensile or compressive, are superimposed on the twisting moment. This type of combined stress torsion test would be particularly useful in establishing the stress criteria for fracture in metal deformation. Bridgman(1) first performed a combined stress torsion test at room temperature with steel and showed large increases in shear strain to fracture with high compressive stresses superimposed on the shear stress. More recently the combined stress torsion test has been used to study ductile fracture during room temperature deformation(2)(3).

The combined stress torsion test was first applied to fracture under hot working conditions during previous research under this project(4). Figure 1 shows the effect of stress state on shear strain to fracture for Inconel 600 tested at various temperatures. The stresses plotted as σ_{max}/τ_{max} represent the largest values of normal and shearing stress applied during the test, assuming that they act on a plane normal to the cylinder axis. Usually this is the initial axial stress and the shearing stress corresponding to the peak in the torque-twist curve. Because the complete analysis of stress in a plastic thin-wall cylinder of short gage length with elastic constraints at the shoulders is not known for combined torque and axial load it was not possible to calculate the maximum principal stress and the maximum shear stress. Nevertheless, the data in Figure 1 show a strong influence of compressive stress in increasing the ductility during hot working.

More recently the combined stress torsion test has been used to study in detail the fracture mechanisms in warm work and hot work in pure nickel(5). It has also been used effectively to study the hot workability of the complex superalloys Waspaloy and Inconel 718 and to correlate their workability with extrusion conditions(6).

STRESS STATE AND DEFORMATION IN COMBINED STRESS TORSION TEST

Since the tensile component of hydrostatic stress promotes the initiation of fracture at sites of structural irregularity while a compressive hydrostatic component suppresses crack growth, it is apparent that a better understanding of the stress distribution in the gage length of the combined stress torsion test would greatly increase its usefulness.

In most previous work utilizing this test(1)(4)(6) only the axial and torsional shear stresses were considered. These were taken to be uniformly distributed over the cross-section and are given by

$$\sigma_Z = \frac{F}{2\pi \bar{r} t} \qquad \text{(Axial Stress)}$$

$$\tau_{Z\theta} = \frac{T}{2\pi \bar{r}^2 t} \qquad \text{(Torsional Stress)} \qquad [1]$$

where F = axial force (lbs.)

T = torque (in-lbs.)

$\bar{r}$ = mean radius (in.)

t = wall thickness (in.)

See Figure 2 for the typical geometry of the test specimen gage length

A notable exception to this is an analysis(3) which concludes that, in addition to the stresses in Equation [1], a circumferential stress exists, given by

$$\sigma_\theta = \sigma_Z - \frac{2\tau_{Z\theta}}{\bar{r}\Delta\theta/\Delta\ell} \qquad [2]$$

where $\Delta\theta/\Delta\ell$ is the increment of twist per change in gage length.

The above analysis is based on the observation that the mean radius of the gage section of the specimens tested does not change during the test. This behavior, however, is not typical of all torsion specimens. Furthermore, the distribution of stresses is not found.

In earlier work by another investigator(7), the radial distribution of stresses in a solid bar under torsion and tension were found using the principle of minimum work. These results, however, cannot be extended to hollow torsion specimens.

Ideally, to establish the radial distribution of stresses and the transiton from plastic to elastic deformation at the notch shoulders, an exact elastic-plastic analysis is required. In the following, a less sophisticated approach to the problem is presented which is based on an approximation of the deformation in the gage length. Nevertheless, the analysis is sufficiently accurate to provide an insight into the nature of the distribution of stresses and the influence of the gage section geometry on the stresses.

It has previously been reported(1), and observed in the present tests as well, that the radial expansion or contraction of the gage section under torsion and axial load is nearly uniform along the gage length. Therefore, as a first approximation, the gage section can be considered as a hollow cylinder undergoing uniform twist and extension or compression with accompanying radial contraction or spread. The shoulders at each end of the gage length act as rigid ends partially constraining radial deformation. This constraint develops radial shear stresses at each end of the gage length, as depicted in Figure 3.

Based on these assumptions and the incompressibility condition for plastic deformation, the radial deformation rate is given by

$$\dot{u} = -\dot{\varepsilon}_z(r^2-r_n^2)/2r \qquad [3]$$

where $\dot{\varepsilon}$ = axial strain rate

r = radial coordinate

r_n = neutral radius (position with no deformation)

The concept of the neutral radius is introduced since simultaneous outward spread of the outer surface and inward spread of the inner surface is observed in some tests, indicating that there is no displacement at some internal point.

Two previous studies using hollow cylindrical specimens indicate the extent of radial constraint provided by the shoulders and serve as bounds on the type of stress states to be expected in axial stress-torsion tests. First, the long, thin-walled tubes used by Taylor and Quinney(8) in their studies of yielding under combined stresses are not subject to radial constraint and the deformation is completely in one direction with the neutral radius at the cylinder axis ($r_n = o$). As a result, the radial and circumferential stresses are zero and the axial and torsional stresses are given by Equation [1]. This stress state would not be expected in axial stress-torsion tests except for those with long, thin-wall gage sections.

Second, tubes with a circular notch tested under axial loads by Bridgman(9) essentially have no gage length but the gage section is subject to full constraint by the material outside the notch. In this case the diameter does not change during the test, and the neutral radius is the mean radius ($r_n = \bar{r}$). The stresses in the notch given below

$$\sigma_r = \sigma_{Za} \ell n[1 + \frac{a}{2R}(1 - x^2/a^2)]$$

$$\sigma_\theta = \sigma_r + \sigma_{Za}/2 \qquad [4]$$

$$\sigma_Z = \sigma_r + \sigma_{Za}$$

where $2a$ = wall thickness, t (in.)

R = notch radius (in.)

x = distance measured from center of tube wall (in.)

σ_{Za} = axial stress at each edge (psi)

This stress state is characterized by a nearly-parabolic radial stress distribution, while the circumferential and axial stresses have the same distribution superimposed on uniform stresses $\sigma_{Za}/2$ and σ_{Za}, respectively. Stresses of this nature would be approached in specimens with very small gage lengths.

The stress state in an actual axial stress-torsion test can be expected to lie somewhere between the two extremes described above, depending on the gage length and wall thickness of the specimens.

ANALYSIS

Returning to the expressions for the assumed deformation, Equation [3], the radial and circumferential strain rates become

$$\dot{\varepsilon}_r = d\dot{u}/dr = -\dot{\varepsilon}_Z(1 + r_n^2/r^2)/2$$

$$\dot{\varepsilon}_\theta = \dot{u}/r = -\dot{\varepsilon}_Z(1 - r_n^2/r^2)/2 \qquad [5]$$

Substituting these expressions in the Levy-Mises equations, and rearranging, the stress differences are found:

$$\sigma_\theta - \sigma_r = \frac{2}{3}\frac{\dot{\varepsilon}_Z}{\lambda}\frac{1}{r'^2}$$

$$\sigma_r - \sigma_Z = -\frac{\dot{\varepsilon}_Z}{\lambda}(1 + \frac{1}{3r'^2}) \qquad [6]$$

$$\sigma_Z - \sigma_\theta = \frac{\dot{\varepsilon}_Z}{\lambda}(1 - \frac{1}{3r'^2})$$

where $r' = r/r_n$

and $\lambda = \dot{\bar{\varepsilon}}/\bar{\sigma}$, ratio of effective strain rate to effective stress at the current value of total effective strain

For plastic flow, a yield criterion must also be satisfied. The von Mises yield criterion will be used

$$(\sigma_\theta - \sigma_r)^2 + (\sigma_r - \sigma_Z)^2 + (\sigma_Z - \sigma_\theta)^2 + 6\tau_{Zr}^2 + 6\tau_{Z\theta}^2 = 2Y^2$$

where Y is the flow stress of the material in simple tension.
Substituting the expressions for stress differences into this yield criterion

$$(1 + \frac{1}{3r'^4})^{1/2} \frac{\dot{\varepsilon}_Z}{\lambda} = (Y^2 - 3\tau_{Z\theta}^2 - 3\tau_{Zr}^2)^{1/2} \qquad [7]$$

Considering the right side of Equation [7] as a reduced effective yield stress, σ_e, the equations for stress differences can now be written as

$$\begin{aligned} \sigma_\theta - \sigma_r &= \frac{2}{\sqrt{3}} \sigma_e/(3r'^4 + 1)^{1/2} \\ \sigma_r - \sigma_Z &= -\frac{\sigma_e}{\sqrt{3}} (3r'^2 + 1)/3r'^4 + 1)^{1/2} \\ \sigma_Z - \sigma_\theta &= \frac{\sigma_e}{\sqrt{3}} (3r'^2 - 1)/(3r'^4 + 1)^{1/2} \end{aligned} \qquad [8]$$

To establish the expressions for the individual stresses the first of Equation [8] is substituted into the equation for radial equilibrium

$$\sigma_\theta - \sigma_r = r(\frac{\partial \sigma_r}{\partial r} + \frac{\partial \tau_{Zr}}{\partial Z}) = \frac{2}{\sqrt{3}} \sigma_e/(3r'^4 + 1)^{1/2} \qquad [9]$$

Before this equation can be integrated to find σ_r, the variation of σ_e and τ_{Zr} must be specified. σ_e varies with total effective strain and the torsional shear stress, both of which will be constant for large strains. Since large strains are involved in the tests, σ_e will be considered constant. τ_{Zr} is the radial shear stress which develops because of the constraint supplied by the shoulders at each end of the gage section. The distribution and magnitude of the radial shear stress is unknown, but, since it is of equal magnitude and opposite sign at each end of the gage section, the axial gradient will be taken as constant

$$\frac{\partial \tau_{Zr}}{\partial Z} = 2\tau/\ell \qquad [10]$$

where τ = radial shear stress at each end

ℓ = gage length

The distribution of the radial shear stress at each end must be such that the direction of the shear stress opposes the direction of the radial spread. Two different distributions are considered:

(a) Constant radial shear stress

$$\tau = \begin{cases} \mp k \text{ for } r_i < r < r_n \\ \pm k \text{ for } r_n < r < r_o \end{cases} \qquad [11a]$$

where r_i, r_o = inside, outside radii

Upper sign for axial compression.

Lower sign for axial tension.

(b) Since the radial shear stress is proportional to $\frac{\partial u}{\partial z}$ which is zero at the neutral radius and has maximum values at the inner and outer surfaces, the radial shear stress is probably more accurately represented by a linear function

$$\tau = \mp k \left\{ \frac{r - r_n}{r_n} \right\} \qquad [11b]$$

Upper sign for axial compression.

Lower sign for axial tension.

These shear stress distributions are shown in Figure 3.

Using Equations [10] and [11] and assuming σ_e is constant, Equation [9] can be integrated to give

$$\sigma_r = \frac{\sigma_e}{\sqrt{3}} \ln(R_i/R) \mp \frac{2kr_n}{\ell} \begin{cases} \text{(a)} \begin{cases} r' - r_i' \text{ for } r_i < r < r_n \\ 2 - r' - r_i' \text{ for } r_n < r < r_o \end{cases} \\ \text{(b) } r' - r_i' - \frac{1}{2}(r'^2 - r_i'^2) \end{cases} \qquad [12]$$

where $R = (1 + (1 + 3r'^4)^{1/2})/r'^2$

At this point the radial stress can be calculated if the magnitude of the radial shear stress and the neutral radius, k and r_n, are known. Neither quantity is known, but a relationship between them can be obtained by applying the boundary condition $\sigma_r = 0$ at the outside radius

$$\frac{\sigma_e}{\sqrt{3}} \ln(R_i/R_o) = \pm \frac{2kr_n}{\ell} \begin{cases} \text{(a)} \begin{cases} r_o' - r_i' \text{ if } r_n < r_i \\ 2 - r_o' - r_i' \text{ if } r_i < r_n < r_o \end{cases} \\ \text{(b) } r_o' - r_i' - \frac{1}{2}(r_o'^2 - r_i'^2) \end{cases} \qquad [13]$$

The variation of the magnitude of the radial shear stress k with neutral radius is shown in Figure 4. It is evident that when the neutral radius is zero the radial shear stress is zero (free radial deformation). As the neutral radius approaches the mean radius, the shear stress becomes unbounded (full constraint of radial deformation). Furthermore, for a given value of shear stress, as the gage length ℓ decreases, the neutral radius approaches the mean radius, while for increasing ℓ the neutral radius approaches zero. This result is consistent with the free radial deformation observed in the long, thin tubes used by Taylor and Quinney(8) and the fully-contrained deformation in Bridgman's notched tubes under axial load(9).

To eliminate the problem presented by this unknown shear stress magnitude, the factor $2kr_n/\ell$ is eliminated in Equation [12] by using Equation [13], giving

$$\frac{\sigma_r}{\sigma_e/\sqrt{3}} = \ell n(R_i/R) - \ell n(R_i/R_o) \begin{cases} \text{(a)} \begin{cases} (r' - r_i')/(r_o' - r_i') \text{ for all } r \text{ if } r_n < r_i \\ (r' - r_i')/(2 - r_o' - r_i') \text{ for } r < r_n \\ (2 - r' - r_i')/(2 - r_o' - r_i') \text{ for } r > r_n \end{cases} \text{if } r_n > r_i \\ \text{(b)} \quad r' - r_i' - 1/2(r'^2 - r_i'^2)/r_o' - r_i' - 1/2(r_o' - r_i'^2) \end{cases} \qquad [14]$$

Thus, if r_n is known, the radial stress σ_r can be calculated.

Under the assumptions described previously the neutral radius can be calculated from Equation [3] if measurements of the deformation of the gage section are made.

$$r_n = r_o\left(1 - 2\,\frac{\ell}{\Delta\ell}\,\frac{\Delta d_o}{d_o}\right)^{1/2} \qquad [15]$$

where $\Delta\ell$, Δd_o are change in gage length and outside diameter, respectively.

The following procedure can now be used to calculate the stresses in the axial stress-torsion test:

(i) From measurements of the change in gage length and change in outside diameter during the test, calculate the neutral radius from Equation [15].

(ii) Calculate the radial stress distribution from Equation [14], using both assumed radial shear stress distributions.

(iii) Calculate the axial and circumferential stress distributions from Equation [8].

This procedure was used to calculate the stress distributions in torsion specimens of various gage lengths for deformation at room temperature.

EXPERIMENTAL RESULTS AND CALCULATIONS

Test were conducted at room temperature on torsion specimens of Inconel 600 with gage lengths of 1/4-, 1/8-, 1/16- and 1/32-inch. The material was in the as-received hot rolled condition with a grain size of approximately .01 mm. For each gage length, three specimens were tested in torsion, one each at no axial load, high compressive axial load, and high tensile axial load. The axial loads were applied such that the average axial stress was one-half the yield stress of the material.

The tests were conducted at low strain-rate ($\sim .01 sec^{-1}$) so that the outside diameter and gage length could be measured as the test progressed. The change of outside diameter with twist is shown in Figure 5 for the tests with axial load. Also shown in the figure is the change in diameter which would occur in the two extreme cases: $r_n = 0$ and $r_n = \bar{r}$. The deformation for the 1/4- inch specimens is nearly that for free radial deformation ($r_n = 0$), but the deformation of the 1/32-inch specimens is less than that for $r_n = \bar{r}$ (full constraint of radial deformation). This indicates that the plastically-deforming material which contributes to the radial deformation exceeds the amount in the gage section and the region of plastic deformation extends into the notch shoulders.

Therefore, the deformed specimens were cut longitudinally and microhardness measurements were made to determine the extent of plastic deformation into the notch shoulders. The transition between plastic and non-plastic material is gradual, but the boundary of the plastic deformation region for specimens of all gage lengths is shown in Figure 6. Plastic deformation in the 1/4- inch specimens extends into the shoulders very little, but the penetration increases substantially as the gage length decreases. In fact, the actual gage length (length of plastic deformation) in the 1/32- inch specimens is more than three times the geometric gage length. Now when the actual gage length is used in Equation [15], the line corresponding to $r_n = \bar{r}$ in Figure 5 is less than that measured for the 1/32- inch specimens. It should be pointed out that even though the plastic deformation boundary is curved, the ensuing radial variation in axial deformation is small compared to the overall axial deformation so that the original assumption of uniform axial strain holds.

With the actual values of the gage length determined in the microhardness tests and the measured values of radial deformation, the procedure outlined above was used to calculate the stress distributions in the axial sttess-torsion specimens with geometric gage lengths of 1/4-, 1/16- and 1/32- inch. The results of these calculations are shown in Figure 7. For comparison, the stresses in the long, thin-

walled tubes used by Taylor and Quinney(8) and the notched cylinders used by Bridgman(9) are included. It can be seen that the stresses exhibit a peak which increases in magnitude as the gage length decreases. The hydrostatic stress, plotted as the dotted line in Figure 7, also exhibits a peak which increases as the gage length decreases, even though the average value of the hydrostatic stress increases very little.

If hydrostatic pressure suppresses crack propagation, it would be expected from the above results that cracks which form at the outer surface of small gage length compression-torsion tests will not grow readily through the wall because of the increased hydrostatic pressure within the wall. On the other hand, cracks forming in large gage length specimens will not be retarded because the hydrostatic pressure is nearly constant through the wall. The converse would be expected in tension-torsion specimens. The high hydrostatic tension peak in small gage length specimens would promote crack formation more readily than the nearly uniform hydrostatic stress in large gage length specimens.

Since the point of maximum torque during a torsion test has been shown previously to coincide with the initiation of fracture(4), the shear strain at maximum torque can be used as a measure of strain to failure. For room temperature deformation this is close to the strain to complete fracture. To determine the effect of gage length, and thus hydrostatic stress, on crack growth during deformation, the shear strain at maximum torque is plotted as a function of gage length for the room temperature tests on Inconel 600 described above. The shear strain at maximum torque was calculated from

$$\gamma_{TM} = \theta r/\ell$$

θ = angular rotation at maximum torque (radians)
r = outside radius at maximum torque (in.)
ℓ = actual gage length as determined by hardness tests on deformed specimens (in.)

The results plotted in Figure 8 show a sharp increase in fracture strain in specimens of small gage length with axial compression. The decrease in fracture strain in specimens with axial tension is not nearly as large. Similar results have been observed in previous work on the combined stress torsion test(3)(4), i.e., for a given magnitude of axial stress the increase in fracture strain due to axial compression is much greater than the decrease in fracture strain due to axial tension (see Figure 1).

ELEVATED TEMPERATURE TESTS

An attempt was made to apply the results of the preceding analysis to axial stress-torsion tests at temperatures in the hot working range. In a program similar to the room temperature tests, specimens of various gage lengths were tested in pure torsion, torsion-tension and torsion-compression at 1800°F. To facilitate measurement of the radial deformation and change in gage length, the tests were performed by repeated cycles of heating to 1800°F, twisting through about 30° of rotation at a strain rate of .01sec^{-1}. The specimens were then quenched in water to room temperature, and measurements were made of diameter and length of the test section. However, during the tests the gage sections became severely distorted and the deformation along the gage length was highly non-uniform. In addition, large deviations from the preset axial load occurred as twisting progressed. In the pure torsion tests, the gage section contracted a large amount, inducing a tensile axial force. To maintain the desired axial load, it was necessary to displace the tail stock during the test to compensate for the change in gage length.

Since this mode of deformation was not accounted for in the analysis described above, the analytical results cannot be applied to the high-temperature tests. Since 1800°F is in the hot working region for Inconel where extensive r-type cavity formation and link-up will occur(4)(5) and where high-temperature restoration processes such as recrystallization and grain growth will be active, it is not surprising that well behaved deformation modes were not observed. More extensive research over a wider range of specimen geometry, especially with larger diameter specimens, is required to determine the possibility of extending this stress analysis to the high temperature hot working region.

AXIAL STRAIN DURING TORSION

In pure torsion of cylindrical specimens, the material in the gage section is subjected to simple shear and no normal strains would be expected. However, in the room temperature tests described previously small axial elongation (~10%) were observed, even though a pure twisting torque was applied to the specimen. In the high temperature tests, large contractions of the gage section were observed during twisting.

The axial elongation found for the room temperature torsion tests is plotted in Figure 9 for each of the pure torsion specimens. The elongation varies linearly and the ratio of axial strain to shear strain is indicated for each curve. Similar results have been reported by other investigators(10)(11).

Axial elongations during twist in room temperature tests should be explainable on the basis of the anisotropy of the material. In the torsion test specimens, a preferred orientation is developed in the circumferential direction due to the progressing twist. This results in a differential in workhardening between the torsional and axial modes of deformation. According to an analysis by Hill(12), for large twist an axial elongation will develop if $\sqrt{3}$ x torsional shear stress is greater than the axial yield stress. For an isotropic material, these will be equal.

In the high-temperature (1800°F) torsion tests severe contraction of the gage section occurred during twisting, as shown in Figure 10. This behavior has been observed in other hot torsion tests in the hot working region (13)(14) using solid torsion specimens. In order to extend the analysis of the stress state in the hot torsion test to account for these effects it will be necessary to identify the mechanisms responsible for these length changes. It would seem possible to correlate the onset and magnitude of the length changes with the fracture and restoration processes occurring at different temperatures and strain rates.

SUMMARY AND CONCLUSIONS

Based on the assumption that the gage section in axial stress-torsion tests undergoes uniform twist as well as uniform axial strain, the stress distributions in the gage section are derived. Calculation of the stresses requires measurement of the radial deformation and extent of the plastic deformation into the notch shoulders. The spread of the plastic region into the notch shoulders increases with decreasing geometric gage length. The radial distribution of stresses exhibits a peak whose amplitude increases with decreasing gage length. In room temperature tests, the fracture strain varies in accordance with the calculated hydrostatic stress.

The analysis of the stresses in the axial stress-torsion test is based on an approximation of the deformation and an assumed distribution of the radial shear stress which partially constrains radial deformation of the material. For each of the two radial shear distributions assumed, the nature of the resulting normal stress distributions is the same. The analytical results thus give a good indication of the variation of the hydrostatic stress with gage length in the axial stress-torsion test. Non-uniform deformation along the gage length and marked changes in length of the specimen preclude the application of this analysis to hot torsion testing without more detailed knowledge of the processes involved.

ACKNOWLEDGMENT

Assistance in carrying out the torsion tests and measurements was provided by L. Shapiro, M. M. Hagerty and D. L. Baty. Discussions on the mechanisms of hot working and deformation were conducted with Professor G. E. Dieter.

REFERENCES

1. P. W. Bridgman, "On Torsion Combined with Compression," Journal of Applied Physics, vol. 14, June 1943, p. 272.

2. S. S. Chang and W. B. Higinbotham, "Comparisons between the Shearing Properties of Alpha Brass as Derived from the Cutting Process and from Static and Impact Torsion Tests," Trans. ASME, sec. B, vol. 82, 1960, pp. 315-323.

3. V. A. Tipnis and N. H. Cook, "The Influence of Stress State and Inclusion Content on Ductile Fracture with Rotation," ASME Paper No. 67-Met 9.

4. G. E. Dieter and E. Shapiro, "Fracture of Metals during Deformation Processing under Conditions of Hot Working," Final Report, contract NOw-66-0207-d, Nov. 30, 1966.

5. E. Shapiro and G. E. Dieter, "Fracture of Metals during Deformation Processing under Conditions of Hot Working," Final Report, contract NOOO19-67-C-0251, April 30, 1968.

6. J. M. Hoegfelt, "Manufacturing Technology for the Extrusion of Superalloy Structural Shapes," Phase II Eng. Report IR8-301, contract AF33(615)-2873, Jan. 1967.

7. A. Nadai, Plasticity, McGraw-Hill Book Co., Inc., New York, 1931, p. 216.

8. G. I. Taylor and H. Quinney, Proc. Royal Soc.(London), vol. 230A, 1931, pp. 323-362.

9. P. W. Bridgman, Studies in Large Plastic Flow and Fracture, Harvard Univ. Press, Cambridge, Mass., 1964, p. 36.

10. H. W. Swift, "Length Changes in Metals under Torsional Overstrain," Engineering, April 4, 1947, p. 253.

11. H. P. Stüwe and H. Turck, "Zur Messung von Fleisskurven in Torsionversuch," Z. Metallkunde, v. 55, No. 11, 1964, p. 699.

12. R. Hill, Plasticity, Oxford University Press, London, 1950, p. 325.

13. D. E. R. Hughes, "The Hot Torsion Test for Assessing Hot-Working Properties of Steels," J. Iron and Steel Inst., March, 1962, p. 214.

14. F. Morozumi, "Study on Hot Workability of Steel," Nippon Kokan Technical Report, v. 4, Feb. 1965, p. 67.

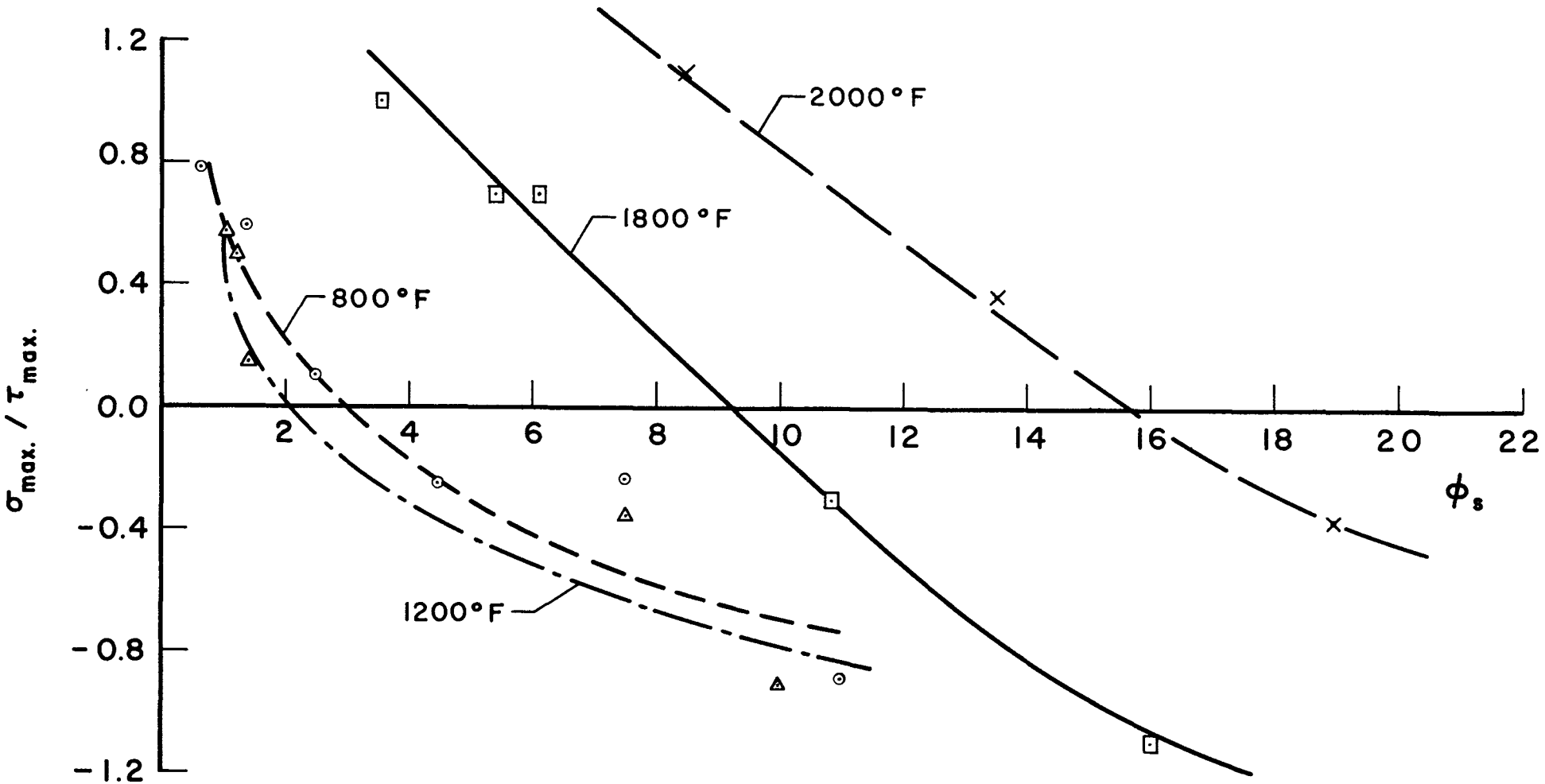

FIG 1. RATIO OF MAXIMUM NORMAL STRESS TO MAXIMUM SHEAR STRESS vs. ϕ_s FOR HOT-ROLLED INCONEL 600

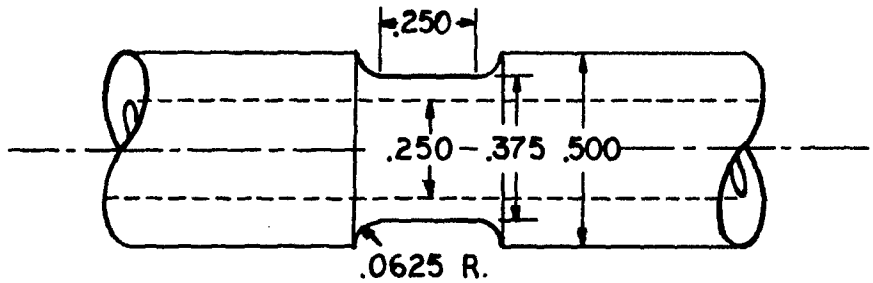

FIG 2. DIMENSIONS OF A TYPICAL GAGE SECTION

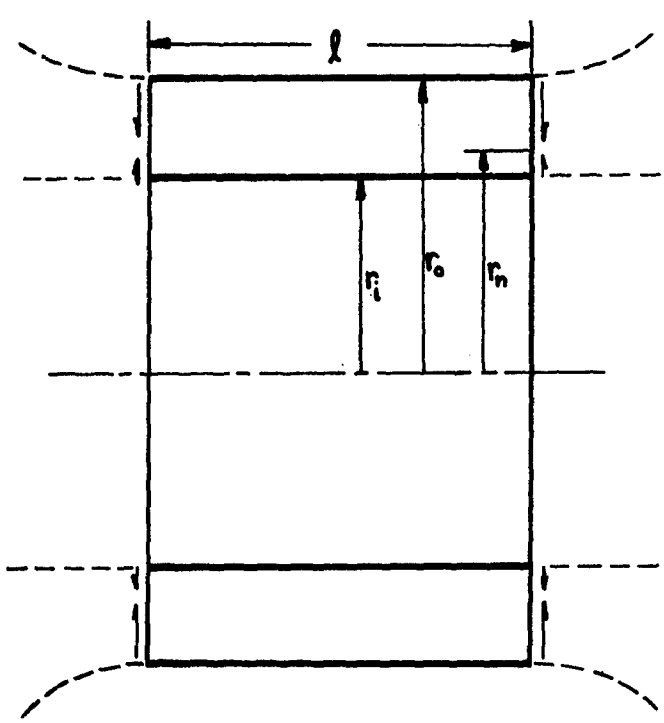

FIG 3. RADIAL SHEAR STRESS AT EACH END OF THE GAGE SECTION. SHEAR DIRECTION SHOWN FOR AXIAL COMPRESSION.

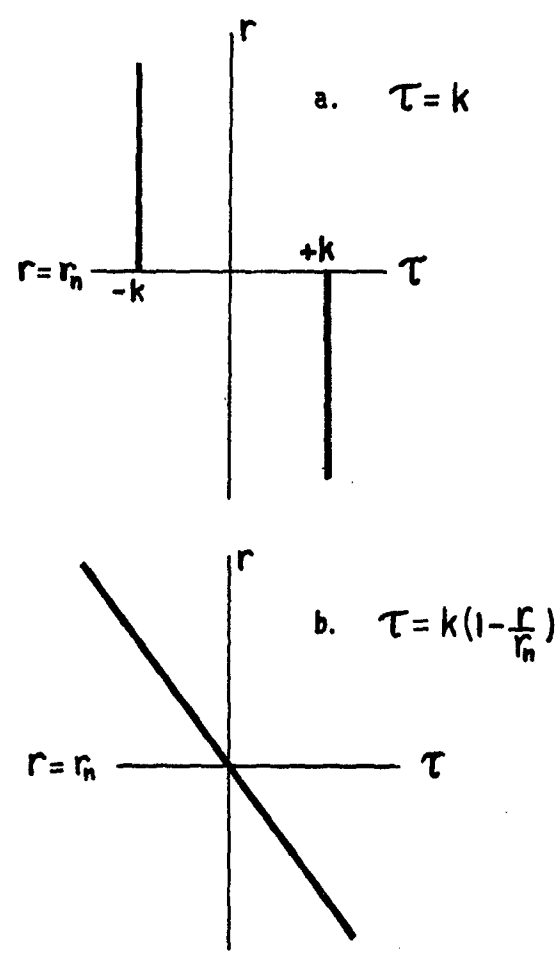

ASSUMED SHEAR DISTRIBUTIONS

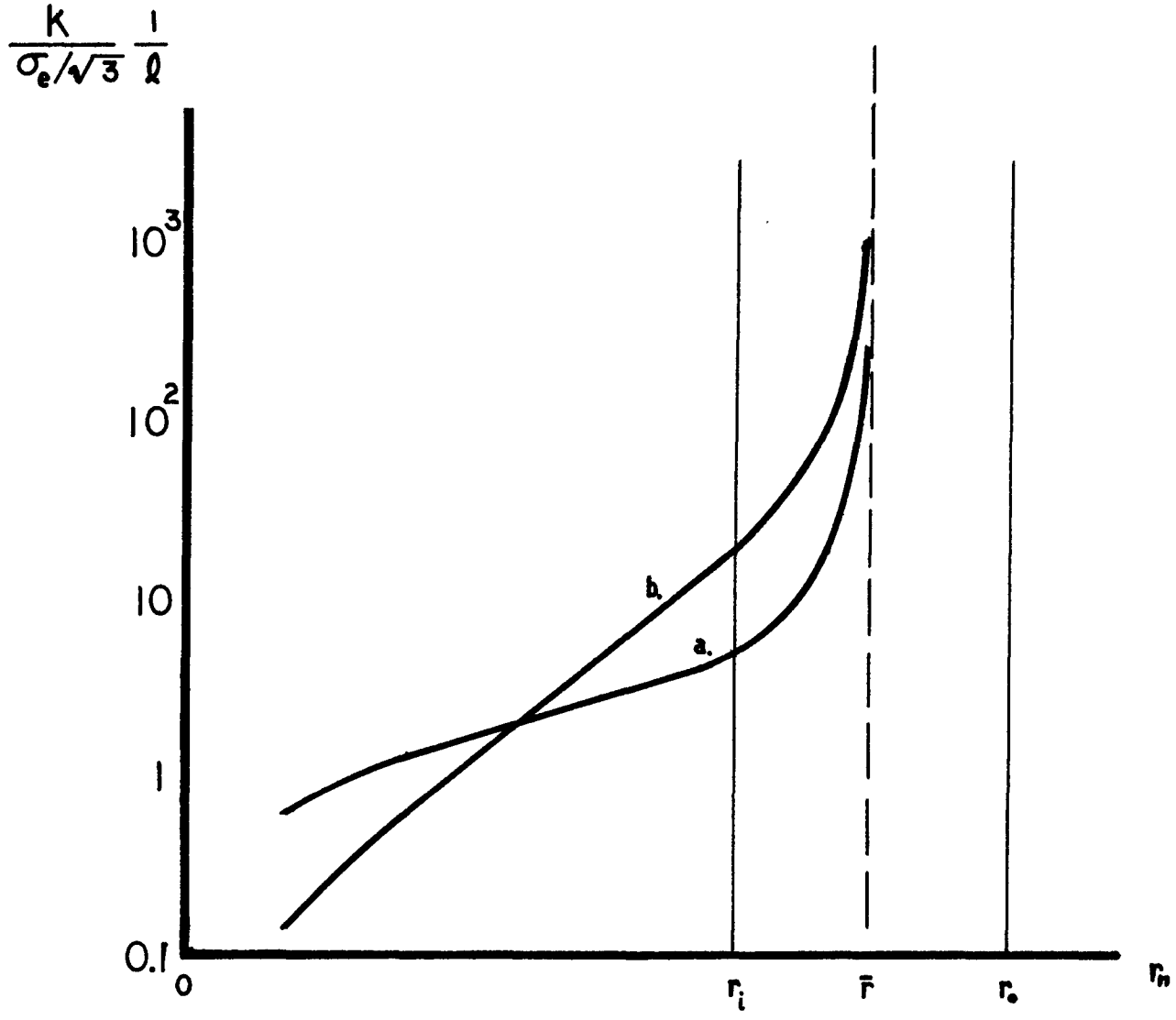

FIG 4. $\frac{K}{\sigma_e/\sqrt{3}}\frac{1}{\ell}$ vs. NEUTRAL RADIUS

FOR THE CASE r_i .125" r_o .1875" $\bar{r}$ .15625"

a. $\tau = K$

b. $\tau = K(1 - r/r_n)$

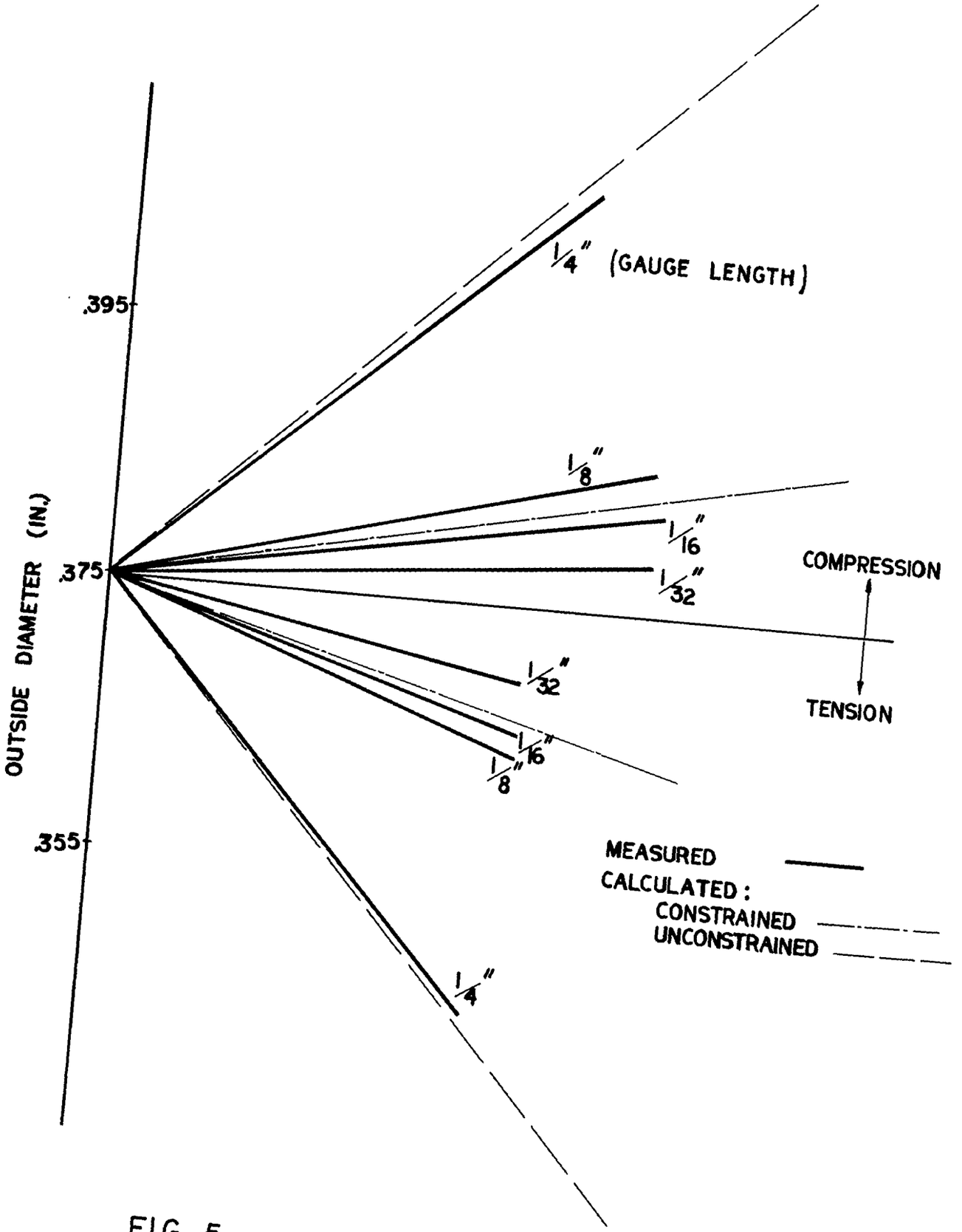

FIG 5. CHANGE IN OUTSIDE DIAMETER WITH ROTATION FOR INCONEL TESTED AT ROOM TEMPERATURE

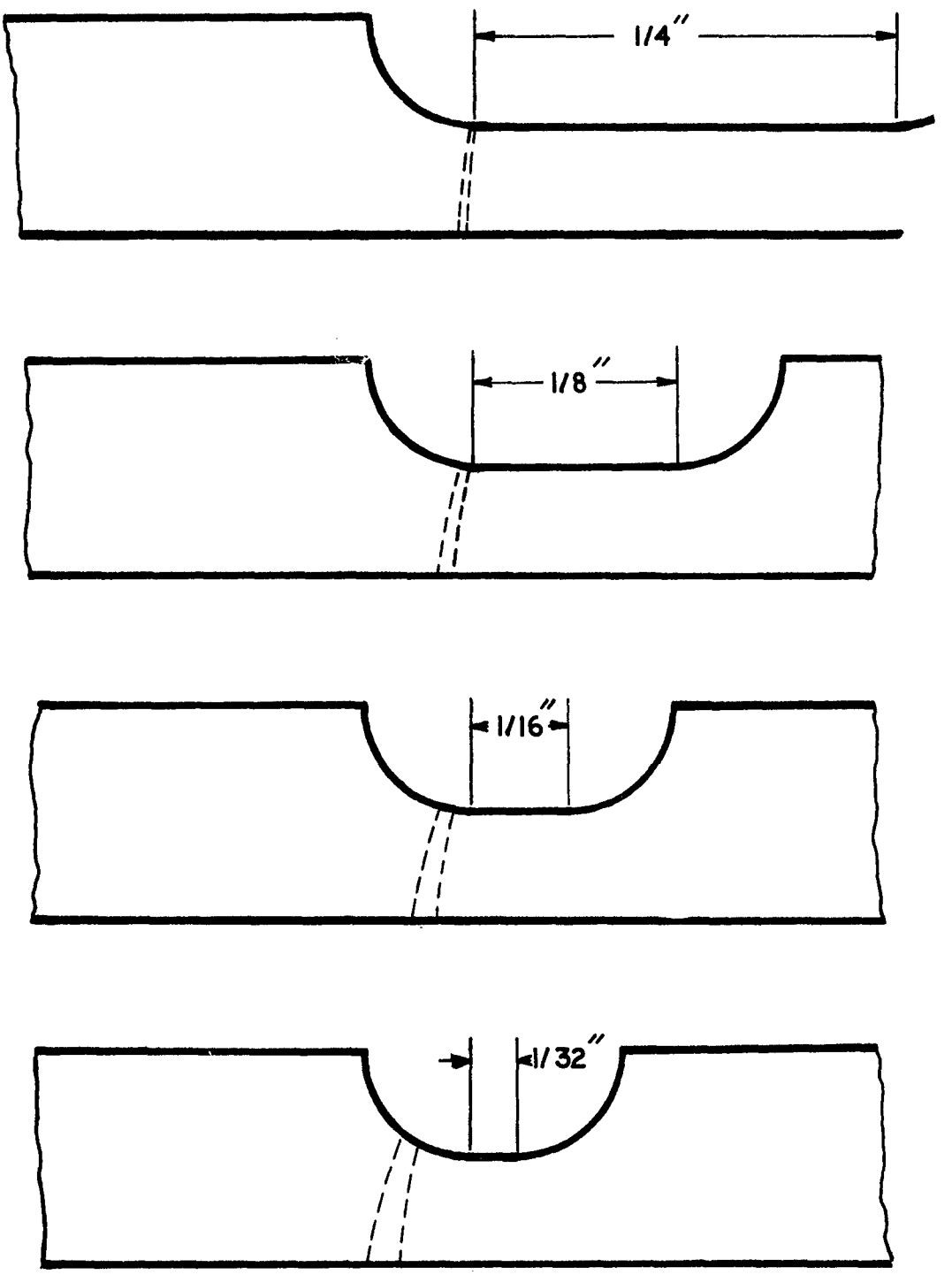

FIG 6. PENETRATION OF THE PLASTIC REGION INTO THE NOTCH SHOULDERS. DASHED LINES INDICATE TRANSITION FROM PLASTIC TO ELASTIC DEFORMATION.

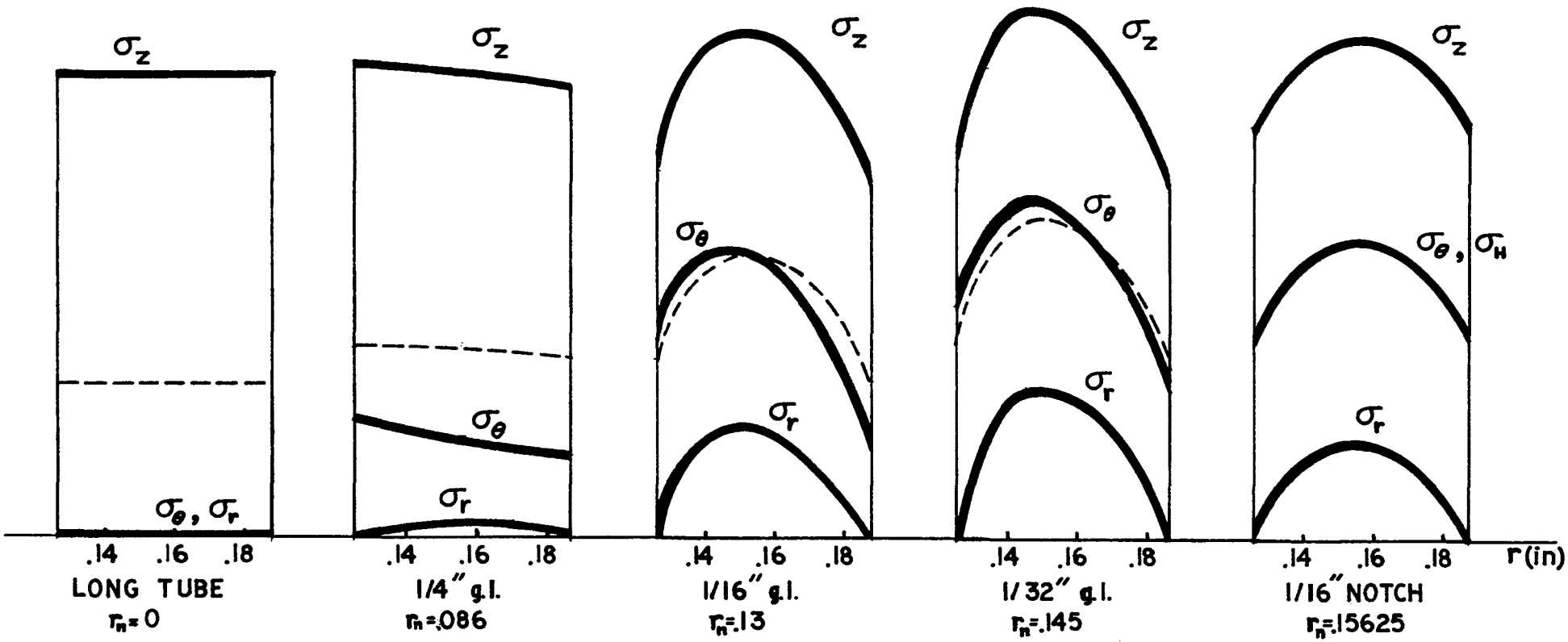

FIG 7. RADIAL DISTRIBUTION OF STRESSES $\sigma_z, \sigma_r, \sigma_\theta$.
HYDROSTATIC STRESS ------

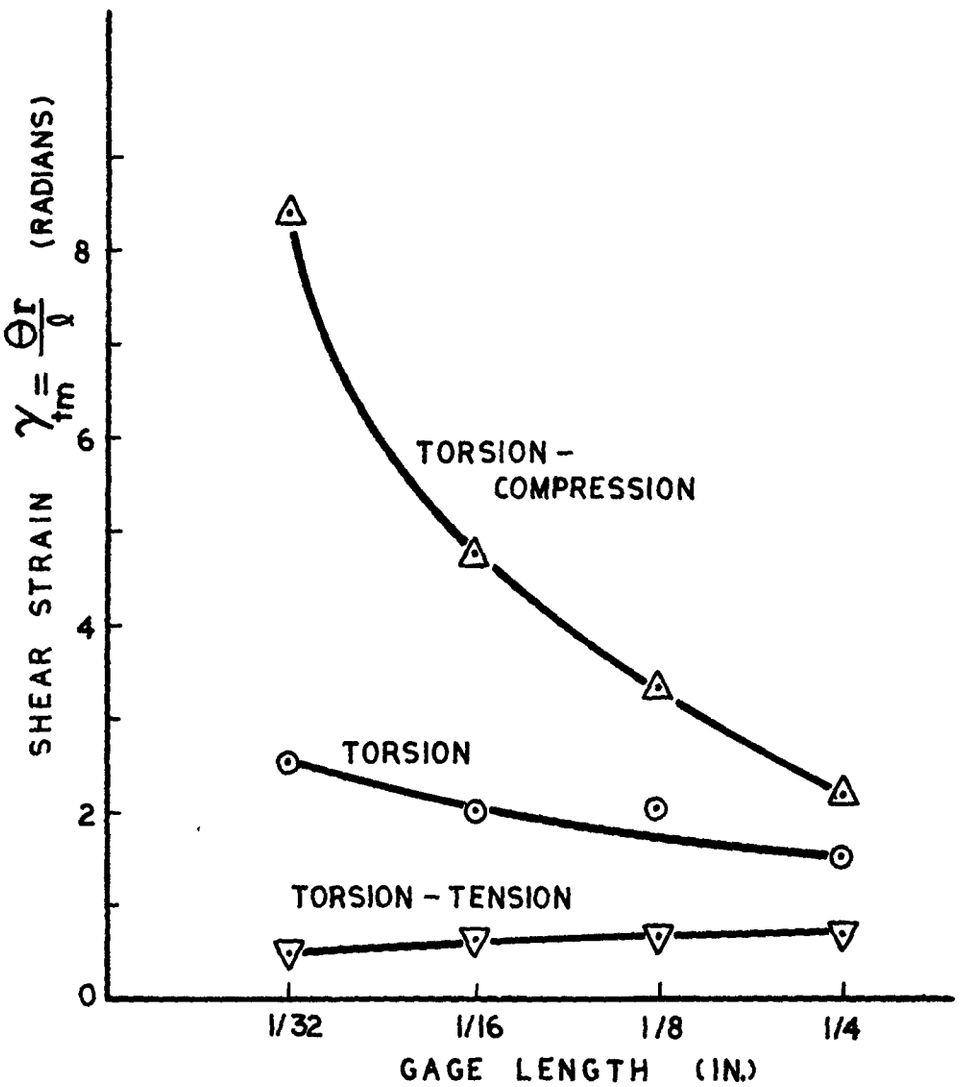

FIG 8. STRAIN AT MAXIMUM TORQUE (ONSET OF FRACTURE) IN ROOM TEMPERATURE TESTS ON INCONEL.

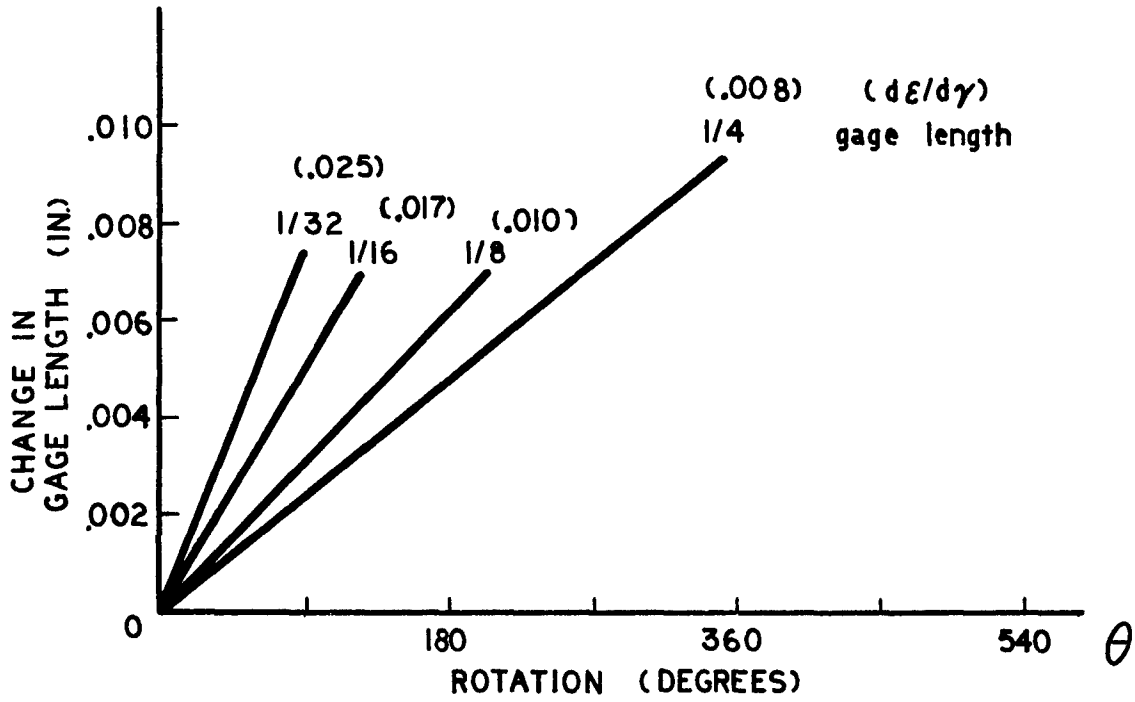

FIG 9. CHANGE IN GAUGE LENGTH WITH ROTATION IN ROOM TEMPERATURE TESTS UNDER PURE TORSION

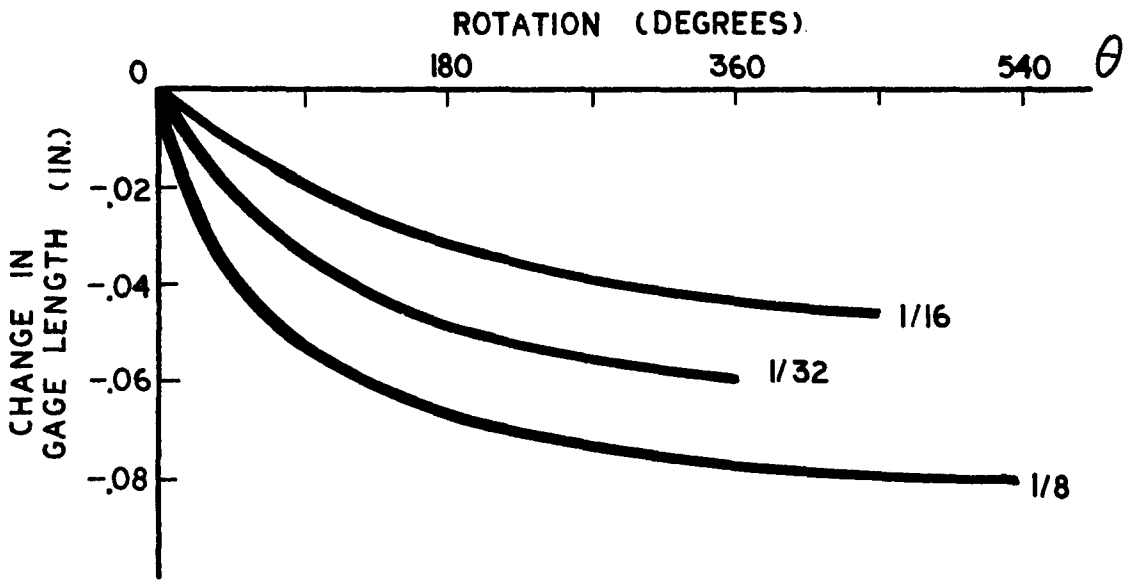

FIG 10. CHANGE IN GAUGE LENGTH WITH ROTATION IN ELEVATED TEMPERATURE TESTS (1800° F.) UNDER PURE TORSION

UNRESTRICTED

Security Classification

DOCUMENT CONTROL DATA - R&D

(Security classification of title, body of abstract and indexing annotation must be entered when the overall report is classified)

1. ORIGINATING ACTIVITY *(Corporate author)* Department of Metallurgical Engineering Drexel Institute of Technology Philadelphia, Pa. 19104	2a. REPORT SECURITY CLASSIFICATION 2b. GROUP

3. REPORT TITLE

Stress State in the Combined Stress Torsion Test

4. DESCRIPTIVE NOTES *(Type of report and inclusive dates)*

Summary Report

5. AUTHOR(S) *(Last name, first name, initial)*

Kuhn, H. A.

6. REPORT DATE	7a. TOTAL NO. OF PAGES	7b. NO. OF REFS
May 24, 1968	26	14

8a. CONTRACT OR GRANT NO.	9a. ORIGINATOR'S REPORT NUMBER(S)
N00019-67-C-0251 b. PROJECT NO. c. d.	9b. OTHER REPORT NO(S) *(Any other numbers that may be assigned this report)*

10. AVAILABILITY/LIMITATION NOTICES

11. SUPPLEMENTARY NOTES	12. SPONSORING MILITARY ACTIVITY
	Naval Air Systems Command Washington, D. C.

13. ABSTRACT

An analysis of the stresses in the axial stress-torsion test is presented by considering the gage section as a cylinder undergoing uniform axial deformation with superimposed torsion. Calculation of the stresses requires measurement of the radial deformation and penetration of the plastic region into the notch shoulders.

The hydrostatic stress exhibits a peak within the wall of the gage section which increases with decreasing gage length. The fracture strain in room temperature tests increases with decreasing gage length when a compressive axial load is applied and decreases slightly with decreasing gage length when a tensile axial load is applied. Severe distortion and large changes in length of the gage section during hot torsion testing prevent application of the analysis to high temperature tests.

DD FORM 1 JAN 64 1473

UNRESTRICTED

Security Classification

14. KEY WORDS	LINK A		LINK B		LINK C	
	ROLE	WT	ROLE	WT	ROLE	WT
Hot twist test Combined stress torsion test						

INSTRUCTIONS

1. ORIGINATING ACTIVITY: Enter the name and address of the contractor, subcontractor, grantee, Department of Defense activity or other organization *(corporate author)* issuing the report.

2a. REPORT SECURITY CLASSIFICATION: Enter the overall security classification of the report. Indicate whether "Restricted Data" is included. Marking is to be in accordance with appropriate security regulations.

2b. GROUP: Automatic downgrading is specified in DoD Directive 5200.10 and Armed Forces Industrial Manual. Enter the group number. Also, when applicable, show that optional markings have been used for Group 3 and Group 4 as authorized.

3. REPORT TITLE: Enter the complete report title in all capital letters. Titles in all cases should be unclassified. If a meaningful title cannot be selected without classification, show title classification in all capitals in parenthesis immediately following the title.

4. DESCRIPTIVE NOTES: If appropriate, enter the type of report, e.g., interim, progress, summary, annual, or final. Give the inclusive dates when a specific reporting period is covered.

5. AUTHOR(S): Enter the name(s) of author(s) as shown on or in the report. Enter last name, first name, middle initial. If military, show rank and branch of service. The name of the principal author is an absolute minimum requirement.

6. REPORT DATE: Enter the date of the report as day, month, year; or month, year. If more than one date appears on the report, use date of publication.

7a. TOTAL NUMBER OF PAGES: The total page count should follow normal pagination procedures, i.e., enter the number of pages containing information.

7b. NUMBER OF REFERENCES: Enter the total number of references cited in the report.

8a. CONTRACT OR GRANT NUMBER: If appropriate, enter the applicable number of the contract or grant under which the report was written.

8b, 8c, & 8d. PROJECT NUMBER: Enter the appropriate military department identification, such as project number, subproject number, system numbers, task number, etc.

9a. ORIGINATOR'S REPORT NUMBER(S): Enter the official report number by which the document will be identified and controlled by the originating activity. This number must be unique to this report.

9b. OTHER REPORT NUMBER(S): If the report has been assigned any other report numbers *(either by the originator or by the sponsor)*, also enter this number(s).

10. AVAILABILITY/LIMITATION NOTICES: Enter any limitations on further dissemination of the report, other than those imposed by security classification, using standard statements such as:

(1) "Qualified requesters may obtain copies of this report from DDC."

(2) "Foreign announcement and dissemination of this report by DDC is not authorized."

(3) "U. S. Government agencies may obtain copies of this report directly from DDC. Other qualified DDC users shall request through _____."

(4) "U. S. military agencies may obtain copies of this report directly from DDC. Other qualified users shall request through _____."

(5) "All distribution of this report is controlled. Qualified DDC users shall request through _____."

If the report has been furnished to the Office of Technical Services, Department of Commerce, for sale to the public, indicate this fact and enter the price, if known.

11. SUPPLEMENTARY NOTES: Use for additional explanatory notes.

12. SPONSORING MILITARY ACTIVITY: Enter the name of the departmental project office or laboratory sponsoring *(paying for)* the research and development. Include address.

13. ABSTRACT: Enter an abstract giving a brief and factual summary of the document indicative of the report, even though it may also appear elsewhere in the body of the technical report. If additional space is required, a continuation sheet shall be attached.

It is highly desirable that the abstract of classified reports be unclassified. Each paragraph of the abstract shall end with an indication of the military security classification of the information in the paragraph, represented as *(TS)*, *(S)*, *(C)*, or *(U)*.

There is no limitation on the length of the abstract. However, the suggested length is from 150 to 225 words.

14. KEY WORDS: Key words are technically meaningful terms or short phrases that characterize a report and may be used as index entries for cataloging the report. Key words must be selected so that no security classification is required. Idenfiers, such as equipment model designation, trade name, military project code name, geographic location, may be used as key words but will be followed by an indication of technical context. The assignment of links, rules, and weights is optional.

DISTRIBUTION LIST

Contract N00019-67-C-0251

Investigation of Fracture of Metals During
Deformation Processing Under Conditions of Hot Working

ADDRESSEE

Commander, Naval Air Systems Command
Department of the Navy
Washington, D. C. 20360
Attn: Mr. W. T. Highberger
Code AIR-52031D

Commander, Naval Air Systems Command
Department of the Navy
Washington, D. C. 20360
Attn: Code AIR-604

Commanding Officer
Air Force Materials Laboratory
Mfg. Technology Division
Wright-Patterson Air Force Base, Ohio 45433
Attn: Mr. H. Johnson (MATB)
Mr. G. Gleen (MATB)

Commanding Officer
Air Force Materials Laboratory
Metals and Ceramic Division
Wright-Patterson Air Force Base, Ohio 45433
Attn: Mr. I. Perlmuter (MAMP)
Mr. V. DePierre (MAMP)

Commanding Officer
Air Force Materials Laboratory
Manufacturing Technology Division
Metallurgical Processing Branch
Wright-Patterson Air Force Base, Ohio 45433
Attn: Mr. C. Cook (MATB)
Mr. M. Gunther (MATF)

Commanding Officer
Air Force Materials Laboratory
Non-Metallic Materials Division
Fluid and Lubricant Materials Branch
Wright-Patterson Air Force Base, Ohio 45433

Director
National Aeronautical and Space Administration
Washington, D. C. 20546
Attn: Mr. M. R. Raring
Code RRM

Headquarters
Army Material Command
AMC-RD-RS-CM
Washington, D. C. 20315
Attn: Dr. P. Kosting

Mr. Stewart Arnold
Assistant Director
Materials Laboratory
Army Materials and Mechanics Research Center
Watertown, Massachusetts 02172

Defense Metals Information Center
Battelle Memorial Institute
505 King Avenue
Columbus, Ohio 43201
Attn: Mr. R. Runck

Dr. W. Rostoker
Professor of Metallurgy
College of Engineering
University of Illinois
P. O. Box 4348
Chicago, Illinois 60680

Dr. G. E. Dieter, Jr.
Head, Department of Metallurgical Engineering
Drexel Institute of Technology
32nd and Chestnut Street
Philadelphia, Pennsylvania 19112

ADDRESSEE

Mr. J. H. Keeler
Manager - Engineering
Lamp Metals & Components Department
General Electric Company
21800 Tungsten Road
Cleveland, Ohio 44117

Professor W. A. Backofen
Associate Professor
Department of Metallurgy
Massachusetts Institute of Technology
77 Massachusetts Avenue
Cambridge, Massachusetts 02139

Dr. M. E. Merchant
Director of Physical Research
Cincinnati Milling Machine Company
Cincinnati, Ohio 45209

Professor N. H. Polakowski
Professor of Mechanical Metallurgy
Illinois Institute of Technology
Chicago, Illinois 60616

Mr. Roger I. Whiteley
Associate Director of the Mechanical Metallurgy Div.
Homer Research Laboratories
Bethlehem Steel Company
Bethlehem, Pennsylvania 18016

Mr. William W. Wood
Project Engineer
Manufacturing Research & Development Department
Ling-Temco-Vought Corporation
Vought Aeronautics Division
P. O. Box 14
Dallas, Texas 75222

Mr. R. E. Machery
Sr. Metallurgical Engineer
Argonne National Laboratory
9700 South Cass Avenue
Argonne, Illinois 60439

University of California
Berkeley, California 94720
Attn: Prof. S. Kobayaski (1)
Prof. Eric Thomsen (1)
Mechanical Engineering Department
University Library (1) (Final Report Only)

Dr. D. C. Drucker
Prof. Mechanical Engineering
Brown University
Providence, Rhode Island 02812

Dr. C. Wistreich
British Iron and Steel Research Association
11 Old Park Lane
London W. 1 England
Via: Mr. W. T. Highberger (Code AIR-52031D)
Naval Air Systems Command
Washington, D. C. 20360

Defense Documentation Center
Cameron Station
Alexandria, Virginia 22314
Via: Commander, Naval Air Systems Command
(Code AIR-604)
Department of the Navy
Washington, D. C. 20360

Chief, Office of Naval Research
Department of the Navy
Washington, D. C. 20390
Attn: Dr. G. Rauch, Metallurgy Branch

ADDRESSEE

U. S. Naval Air Development Center
Aero Materials Department, Johnsville
Warminster, Pennsylvania 18974
Attn: Mr. F. S. Williams, Supt. Metallurgy Div.

Commander, Naval Ships Systems Command
Navy Department
Applied Research Division
Washington, D. C. 20360
Attn: Mr. G. Sorkin (Code SHIP 0342)

Commanding General
Watervliet Arsenal
Benet Laboratories
Watervliet, New York 12189
Attn: Mr. T. Davidson
Dr. R. Weigle

Commanding General
U. S. Army Weapons Command
AMS- WE-RDR
Rock Island, Illinois 61201

Lewis Research Center
National Aeronautics & Space Administration
21000 Brookpark Road
Cleveland, Ohio 44135
Attn: Mr. R. W. Hall
Mail Stop 105-1

Mr. Charles Blankenship
Lewis Research Center, Mail Stop 105-1
National Aeronautics & Space Administration
21000 Brookpark Road
Cleveland, Ohio 44135

Scientific & Technical Information Facility
P. O. Box 5700
Bethesda, Maryland 20014
Attn: NASA Representative
SAK/DL-419

Prof. M. C. Shaw
Head, Mechanical Engineering
Carnegie Institute of Technology
Schenley Park
Pittsburgh, Pennsylvania 15213

Prof. Eric Schmid
11 Physikal Institut
University of Vienna
Strudhofgasse 4
Vienna, IX, Austria
Via: Mr. W. T. Highberger (Code AIR-52031D)
Naval Air Systems Command
Washington, D. C. 20360

Dr. Volker Weiss
Associate Professor of Metallurgy
Syracuse University
Metallurgical Research Laboratories
Building D-6, Collendale Campus
Syracuse, New York 10310

Massachusetts Institute of Technology
Department of Metallurgy
77 Massachusetts Avenue
Cambridge, Massachusetts 02139
Attn: Dr. N. Grant

U. S. Steel Corporation
Research & Technology Division
525 William Penn Place
Pittsburgh Pennsylvania 15219
Attn: Mr. M. W. Lightner, V. P.
Applied Research

Prof. H. Ll. D. Pugh
Department of Scientific and Industrial Research
Materials Group
Plasticity Division
National Engineering Laboratory
East Kilbride, Glassgow, Scotland
Via: Mr. W. T. Higherberger (Code AIR-52031D)
Naval Air Systems Command
Washington, D. C. 20360

ADDRESSEE

General Electric Company
Research and Development Center
Schenectady, New York 12301
Attn: Dr. D. W. Lillie (1)
Dr. H. Rogers (1)
Dr. L. F. Coffin (1)
Metallurgy and Ceramics Research Dept.

Mr. Adolph J. Lena
Product Development Department
Research Center
Allegheny Ludlum Steel Corporation
Brackenridge, Pennsylvania 15014

Mr. Richard Cogan
General Electric Company
Thomsen Engineering Laboratory
Small Engines Department
West Lynn, Massachusetts 01905

Westinghouse Electric Corporation
Research & Development Laboratories
Beulah Road, Churchill Boro
Pittsburgh, Pennsylvania 15235
Attn: Dr. J. Brown

Pressure Technology Corporation
435 Amboy Avenue
Woodbridge, New Jersey 07075
Attn: Dr. A. Bobrowsky, President

Solar Division
International Harvester Company
2200 Pacific Highway
San Diego, California 92112
Attn: Mr. J. V. Long
Director of Research

TRW, Inc.
Materials Laboratory
23555 Euclid Avenue
Cleveland, Ohio 44117
Attn: Dr. Nemy

Dr. O. D. Sherby
Department of Materials Science
Stanford University
Stanford, California 94305

Dr. Robert F. Hockman
Associate Professor
Department of Metallurgy
Georgia Institute of Technology
Atlanta, Georgia 30332

Dr. Frederick N. Rhines
Department of Metallurgy
University of Florida
Gainesville, Florida 32601

Prof. John C. Shyne
Department of Metallurgy
Stanford University
Stanford, California 94305

New England Materials Laboratory
35 Commercial Street
Medford, Massachusetts 02155
Attn: Dr. A. S. Bufford

Commanding Officer
U. S. Naval Ordnance Laboratory
White Oak, Silver Spring, Maryland 20910
Attn: Dr. A. Rozner
Metallurgy Processing Section
Magnetic Materials Division

Prof. N. V. Fairbanks
Department of Metallurgy
West Virginia University
Morgantown, West Virginia 26505

Professor L. V. Colwell
Department of Mechanical Engineering
University of Michigan
Ann Arbor, Michigan 48104

Reactive Metals, Inc.
1000 Warren Avenue
Niles, Ohio 44446
Attn: Technical Director